Density functional study of copper segregation in aluminum

A. Benali [a,b,*], C. Lacaze-Dufaure [a], J. Morillo [b]

[a] CIRIMAT, CNRS UMR 5085, 4 Allée Emile Monso, 31432 Toulouse Cedex 4, France
[b] CEMES, CNRS UPR 8011, 29 rue Jeanne Marvig, 31055 Toulouse Cedex 4, France

Keywords:
(111) Al surface
(100) Al surface
Cu segregation
Density functional calculations
Surface alloys
Surface energy

A B S T R A C T

The structural and electronic properties of Cu segregation in aluminum are studied in the framework of the density functional theory, within the projector augmented plane-wave method and both its local density approximation (LDA) and generalized gradient approximation (GGA). We first studied Al–Cu interactions in bulk phase at low copper concentration (≤3.12%: at). We conclude to a tendency to the formation of a solid solution at $T=0$ K. We moreover investigated surface alloy properties for varying compositions of a Cu doped Al layer in the (111) Al surface then buried in an (111) Al slab. Calculated segregation energies show unstable systems when Cu atoms are in the surface position (position 1). In the absence of ordering effects for Cu atoms in a layer ($x_{Cu}=1/9$ and $x_{Cu}=1/3$), the system is more stable when the doped layer is buried one layer under the surface (position 2), whereas for $x_{Cu}=1/2$ to $x_{Cu}=1$ (full monolayer), the doped layer is more accommodated when buried in the sub-sub-surface (position 3). First stage formation of GP1- and GP2-zones was finally modeled by doping (100) Al layers with Cu clusters in a (111) Al slab, in the surface then buried one and two layers under the surface. These multilayer clusters are more stable when buried one layer beneath the surface. Systems modeling GP1-zones are more stable than systems modeling GP2-zones. However the segregation of a full copper (100) monolayer in an (100) Al matrix shows a copper segregation deep in the bulk with a segregation barrier. Our results fit clearly into a picture of energetics and geometrical properties dominated by preferential tendency to Cu clustering close to the (111) Al surface.

1. Introduction

Aluminum has the capacity to form a very stable oxide. Thus, it leads to high temperature resistant coatings with good resistance to oxidation and corrosion in aggressive environments. It is often alloyed to modify some of its intrinsic properties and various treatments such as precipitation hardening are needed to improve its mechanical properties. The properties of these alloys are not due simply to their chemical composition but are particularly influenced by the involved phases and the alloy microstructure. Copper–aluminum alloys that have good mechanical properties are the most used alloys in the aeronautical field. In microelectronics, Cu/Al joints are widely used in high-direct-current systems to transmit the electric current, and could be used as alternative to Au/Al joint in high-power interconnections and fine-pitch bonding applications due to the very good mechanical, electrical and thermal properties of Cu [1,2]. The oxidation of such alloys can have crucial consequences on the phase properties. We thus want to investigate the first stages of oxidation of copper–aluminum alloys. We need first to study the clean material and understand the Cu–Al interactions. We present here the results of our computations on copper segregation in aluminum. The copper bulk segregation and copper surface segregation are both studied.

During the last two decades several studies on aluminum and its alloys were carried out using first principle calculations. Various bulk phases (perfect phases or in presence of bulk defects) as well as clean Al surfaces were fully investigated. Hoshino et al. [3] showed that the stability of an aluminum based binary alloy Al–M, with a transition metal M, is related to the middle range interactions between the transition atoms, by a strong sp-d hybridization (Al–M). The energy of interaction between two impurities depends strongly on the distance separating them. Using the full potentials Green functions KKR [4,5] for a better description of the crystal defects, they showed that the energy of the copper–copper interaction tends towards 0 eV for $d_{Cu-Cu}>5.5$ Å.

According to the Al/Cu equilibrium phase diagram, at Cu massic concentration lower than 4%, one is in the presence of a solid solution α while the first defined compound is $Al_2Cu-\theta$. Even for low copper concentration, there is a demixion at $T<350$ K and one should thus be in the presence of a two-phase microstructure ($\alpha+\theta$). The formation of the θ phase is also observed at equilibrium when the Cu concentration in the Al matrix is increased. The Cu first precipitates within the bulk into Guinier–Preston-zones [6,7] (GP-zones) and that later transformed to metastable θ' and stable θ phases. Subsequent GP-zones stages are distinguished as GP1- and GP2-zones as they change their structure during annealing. Experimental determination of the atomic structure of the GP-zones is rather difficult owing to

* Corresponding author. CEMES, CNRS UPR 8011, 29 rue Jeanne Marvig, 31055 Toulouse Cedex 4, France.
E-mail addresses: anouar.benali@ensiacet.fr (A. Benali), corinne.dufaure@ensiacet.fr (C. Lacaze-Dufaure), morillo@cemes.fr (J. Morillo).

doi:10.1016/j.susc.2010.10.040

their small size of few nanometers. The GP-zones were first observed with early X-ray experiments suggesting GP1-zones composed of a single (100) Cu layer and a GP2-zone composed of an ordered platelet of two Cu layers separated by three Al(100) layers in the Al matrix [8,9]. Recent results using high-angle annular detector dark-field (HAADF) techniques and diffuse scattering led to unambiguous results confirming single layer platelet zones of copper atoms at irregular distances from each other as the main constitution of GP1-zones and showed the possibility for the existence of multilayer Cu zones [10,11]. Two-layer copper zones are occasionally seen in Al–Cu alloys [12].

Several theoretical studies are also available for some Cu/Al microstructures such as GP-zones in intermetallic compound [13,14]. Using first principles, Wang et al. [15] studied the formation of Guinier–Preston zones in Al–Cu alloys by investigating the atomic structures and formation enthalpies of layered Al–Cu superlattices. They highlighted a supercell total energy decrease with Cu content rise, equivalent to a reduction of spacing of the copper lattice in the superlattice. They considered that the formation and evolution of GP-zones in Al–Cu alloys can be considered as a process of increasing accumulation of copper atoms by means of local coagulation of Cu platelets. Zhou et al. [1] have calculated the structural, elastic and electronic properties of Al–Cu intermetallics from first principle calculations. They obtained polycrystalline elastic properties from elastic constants. They correlated the calculated anisotropy of elastic properties to the electronic nature of Al–Cu intermetallics, as a high charge density is observed in the core region of the Cu atoms, while the density is lower in the interstitial area. Their observations showed a strong directional bonding between the nearest-neighbor Cu atoms and a weak directional bonding between Cu and Al atoms. Vaithyanathan et al. [16] conducted a multiscale modeling study on the growth of $Al_2Cu-\theta$' phase. Wolverton et al. [17–21] produced many first principle studies on the determination of the structural properties and energetics of some Al–Cu phases. Results obtained from a density functional theory (DFT) [22,23] study of $Al_2Cu-\theta$ were in excellent agreement with experimental results, suggesting a good reliability of the calculation methods. Moreover, this study made it possible to highlight the stability of the metastable phase θ' over the stable phase θ at low temperature (T<200 K). The reason for this unexpected stability compared to experimental observations was attributed to a large difference of vibrational entropy of the two polytypes at low temperature.

Experimental techniques have been developed that allow for detailed investigations of surfaces such as Low Energy Electron Diffraction (LEED) [24] and Scanning-Tunneling Microscopy (STM) [25–28]. A necessary condition for a full theoretical interpretation of the results of such experiments is an accurate description of the surface potential and the surface electronic structure [29]. The recent progress in the material sciences has led to the production of surfaces of high purity, and has allowed the design of various structures with desired properties. The understanding of the physicochemical processes of these systems needs a detailed knowledge of the electronic structure of these materials, and in this context surface states play an important role. The ground-state electronic and structural properties of solid surfaces such as the electronic charge density, surface energy, work function or lattice relaxation can now be determined from first principle calculations, inducing a growing interest in accurate theoretical descriptions of the surface properties of solids.

In this paper, Section 2 is a brief description of our computational method. In Section 3 we discuss bulk and clean surface properties. In the first sub-section, we present the results of Al–Cu interactions in bulk phase at different Cu atomic concentrations (0.926%, 1.56% and 3.125%). The calculated negative mixing enthalpies at 0 K, indicate that the alloy will form a solid solution in the absence of any competing ordered phase. The second sub-section is devoted to the clean (111) and (100) Al surfaces. The calculated surface energies are in good agreement with experimental data and other theoretical calculations. Copper segregation at infinite dilution in the (111) and (100) surfaces are studied in Section 4, by the mean of the first, substituting the copper following the (111) plane and then, by the study of the first stage formation of Guinier–Preston zones. In the first sub-sub-section, we discuss the segregation at infinite dilution (1/9 atom of copper in a layer), and then we increase the Cu concentration until a full Cu monolayer in the second sub-section. Cu-doped layers at different Cu concentrations have their geometry and energetics dominated by preferential homoatomic interactions. Finally, we show that Cu clusters in the (100) plane representing the GP-1 zones are more stable when buried one layer under the surface, following the Cu segregation behavior in the (111) plane. There is moreover no tendency to surface segregation of GP-zones at the (100)Al surface.

2. Computational details

All calculations were performed in the framework of DFT with the Vienna *ab initio* simulation package [30–32] (VASP) implementing the projector augmented wave (PAW) method [33,34]. PAW pseudopotentials were defined with ($3s^2 3p^1$) valence electrons for Al and ($3d^{10} 4s^1$) for Cu. For Cu, we checked that it is not necessary to inlcude the *3p* electrons in the valence shell. Both the local density approximation (LDA) [35] and the generalized gradient approximation (GGA) [36] were used to describe the exchange-correlation energy-functional. For LDA functional, we used the formulation proposed by Ceperlay and Alder [35] and parameterized by Perdew and Zunger [37] while for GGA functional, we used the formulation proposed by Perdew, Burke and Ernzerhof, [38] commonly called PBE. Convergence with respect to cutoff E_{cut}, Methfessel-Paxton [39] smearing σ and size of Monkhorst-Pack [40] mesh of *k*-points were carefully checked for each model, in order to have the same energy precision in all calculations (less than 1 meV), leading to the following values: E_{cut} = 450 eV, smearing σ = 0.2 eV. These values, if not otherwise stated, were used in all calculations. The grid of *k*-points was set to (15×15×15) for bulk calculations of pure Cu and Al. For other calculations, the used grids of *k*-points are reported in the corresponding sections. All calculations were done allowing for spin polarization. Atomic positions were relaxed with the conjugate gradient algorithm [41] until forces on moving atoms where less than 0.05 eV/Å.

3. Bulk and surface properties

3.1. Bulk cohesive properties

Bulk fcc Al and Cu were simulated using a primitive trigonal unit cell. Their equilibrium volumes and bulk modulus B_0 were calculated by fitting the total energy of 12 regularly spaced volumes around the

Table 1
Calculated bulk properties for Al and Cu using GGA (LDA) XC functionals in the PAW scheme compared to experimental results and other recent DFT calculations (US = ultrasoft Vanderbilt pseudopotential, PW91 = Perdew Wang 91 XC functional).

Material	Cal. type	a_0 (Å)		B_0 (GPa)		E_c (eV/at.)		Ref.
Al	Experiment	4.05/4.04		76.93/77.30		−3.39/−3.39		[42]/[43]
		LDA	GGA	LDA	GGA	LDA	GGA	
	PAW	3.98	4.04	113.38	67.72	−4.01	−3.43	This work
	US/PW91		4.04		72.05		−3.50	[44]
	All electron		4.04		75.00		−4.07	[45]
	All electron	3.97		80.00		−4.09		[46]
Cu	Experiment	3.61		137.00		−3.49		[42]
		LDA	GGA	LDA	GGA	LDA	GGA	
	PAW	3.52	3.64	185.20	142.00	−4.51	−3.46	This work
	Pseudopotential		3.67		134.00		−3.38	[47]
	Pseudopotential	3.53	3.97	190.00	140.00	−4.75	−3.76	[48]
	All electron	3.52	3.63	192.00	142.00	−4.57	−3.51	[49]

Table 2
$Al_{1-x}Cu_x$ mixing enthalpy per atom, ΔH_m (meV/at.) versus Cu concentration, x in the Cu dilute limit. B: fcc Bravais supercell, P: fcc primitive supercell.

x (%)	0.926	1.56		3.125
N (Al + Cu)	107 + 1	63 + 1		31 + 1
Supercell	3×3×3 fcc B	4×2×2 B	4×4×4 P	2×2×2 B
k points	8×8×8	6×12×12	11×11×11	12×12×12
LDA	−0.85	−1.39	−1.14	−2.78
GGA	−1.31	−2.18	−1.96	−4.4

equilibrium volume to Murnaghan's equation of state [50]. A spin-polarized calculation of an isolated atom was performed using a broken symmetry box of 11×10×9 Å for the determination of the cohesive energy per atom, E_c. For both pure metals, the GGA results are in quite good agreement with experimental data, while LDA overestimates the cohesive energy and bulk modulus, and underestimates the lattice parameter (Table 1), as it does in general for metallic systems [36,51,52]. Our PAW calculations are in overall agreement with previously published all electron calculations (justifying the use of the time-saving pseudopotentials rather than all electron potentials) and other pseudopotential calculations.

The mixing enthalpy per atom, ΔH_m, at $T = 0$ K of the fcc $Al_{1-x}Cu_x$ solid solution in the dilute Cu limit was calculated at three different Cu atomic concentrations ($x = 0.92\%$, 1.52% and 3.12%).

$$\Delta H_m(x) = E_c(\mathrm{Al}_{1-x}\mathrm{Cu}_x) - (1-x)E_c(\mathrm{Al}) - xE_c(\mathrm{Cu}), \quad (1)$$

where $E_c(\mathrm{Al}_{1-x}\mathrm{Cu}_x)$ is the cohesive energy per atom of the solid solution, $E_c(\mathrm{Al})$ and $E_c(\mathrm{Cu})$ are the cohesive energies per atom of the fcc pure Al and Cu phases. The calculations were performed with supercells of different shapes, containing N atoms ($N = 108$, 64, 32), where an Al atom was substituted by one Cu atom. $\Delta H_m(x = 1/N)$ is then defined by:

$$N\Delta H_m(x = 1/N) = E((N-1)\mathrm{Al}, \mathrm{Cu}) - \frac{N-1}{N}E(N\mathrm{Al}) - \frac{1}{N}E(N\mathrm{Cu}) \quad (2)$$

where $E((N-1)\mathrm{Al}, \mathrm{Cu})$ is the energy of the alloy supercell, and $E(N\mathrm{Al})$ and $E(N\mathrm{Cu})$ are the energies of the corresponding pure Al and Cu supercells.[1] The obtained enthalpies of mixing are reported in Table 2, and Fig. 1 (for the GGA results).

Negative mixing enthalpies at 0 K, as presently obtained, mean that the alloy will form a solid solution in the absence of any competing ordered phase. However, this tendency is weak ($\Delta H_m(x) \approx$ meV). Fig. 1 shows that the α solid solution is slightly unstable at 0 K against a demixion in pure Al and the ordered Al_2Cu−θ phase. This is in agreement with the very small, increasing with temperature, extension of the α phase in the Al-Cu phase diagram at intermediate temperatures which, then, results from entropic effects. The almost linear variation of $\Delta H_m(x)$ with Cu concentration shows that, in this concentration range ($x < 3.2$ at.%) the Cu atoms are independent and can be considered as isolated impurities in the Al matrix. The mixing energy can then be expressed as a function of the dilute impurity enthalpy per Cu atom ΔH_{imp}:

$$\Delta H_m(x) = x\Delta H_{imp} \quad (3)$$

[1] For the considered Cu concentrations, the mixing enthalpies are of the order of the meV, so the supercell energies entering in Eq. (2) were calculated with equivalent highly converged conditions: large k-point grids (see table eftab:enthalpy-mix and smaller smearing parameter (0.01 eV) than the one given in Section 2 leading to a 0.05 meV accuracy for the mixing enthalpies.

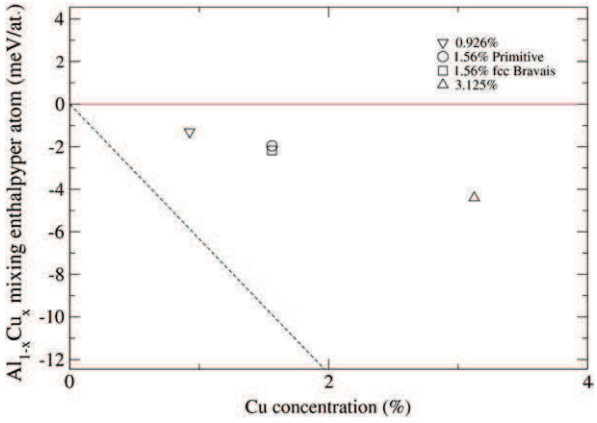

Fig. 1. GGA calculated mixing enthalpies as a function of Cu concentration x. full line: ideal solution, dashed line: line from E_c(Al) to the formation energy of the $Al_2Cu-\theta$ phase.

where the dilute impurity enthalpy per Cu atom is defined by:

$$\Delta H_{imp} = \lim_{x\to 0}\left(\frac{1}{x}\Delta H_m(x)\right) = \mu_{Cu}(x\to 0) - \mu_{Cu}(x=1) = \mu_{Cu}(x\to 0) - E_c(\mathrm{Cu}) \quad (4)$$

where $\mu_{Cu}(x)$ is the chemical potential or partial enthalpy per atom of Cu in the Al–Cu alloy at concentration x.

Table 3 shows that our ΔH_{imp} values deduced from Eq. (4) are in very good agreement with previously calculated ones [19]. The 10–20 meV differences between our results with the Bravais supercell, the primitive supercell, and the results of Wolverton et al. [19] can be attributed to small differences in the parameters controlling the accuracy of thecalculation (cutoff, smearing and k-point grid). Thus, ΔH_{imp} can be evaluated as -130 ± 10 meV from the GGA calculations. Nevertheless, the constant value (within 3 meV), obtained with the Bravais supercell for the three concentrations shows unambiguously that the Cu atoms are truly independent in the studied concentration range since all three calculations were performed with exactly the same accuracy.

3.2. Al (111) and (100) surfaces

Surface phenomena, like adsorption or segregation, can be theoretically studied in slab geometry with periodic boundary conditions. In order to reach low surface concentrations (of adsorbate or segregated atoms) one has to use large surface supercells, which implies to use the thinnest possible slabs without loss of accuracy. To do so, we adopted an asymmetric (AS) slab geometry: one of the surface regions (referred as the top surface) is devoted to the segregation study and is thus free to relax, whereas the other one (referred as the bottom surface) is fixed at the bulk crystal geometry. In this asymmetric configuration the surface energy σ can be obtained from the following expressions of the linear variations (at large n) of the unrelaxed E_{urlx} and relaxed E_{rlx} total

Table 3
Dilute impurity enthalpy per solute Cu atom ΔH_{imp} (meV) in $Al_{1-x}Cu_x$ deduced from Eq. (4) with the fcc Bravais supercells. B: fcc Bravais supercell, P: fcc primitive supercell.

x (%)	0.926		1.56		3.125		
	LDA	GGA	LDA	GGA	LDA	GGA	Cal. type
B	−92	−141	−89	−140	−89	−141	PAW
P			−73	−125			PAW
			−80		−100		US[1]
				−120			PAW[1]

Table 4
Calculated properties of the (111)Al surface and comparison to other calculations and known experimental values. Calculations (Ps: pseudo, AE: all electron) and number of layers n (S, AS: symmetric or asymmetric slab). Calculations and experiment (LEED = Low Energy Electron Diffraction): σ_{urlx}(eV/at.) unrelaxed and σ(eV/at.) relaxed surface energy, Φ(eV) work function and Δ_{ij}(%) relative interlayer distances (see text).

	n	σ_{urlx}	σ	Φ	Δ_{12}	Δ_{23}	Δ_{34}	Ref.
PAW/GGA	13 (AS)	0.347	0.346	4.012	+0.522	−0.552	+0.460	This work
PAW/GGA	13 (S)		0.359	4.013	+0.498	−0.528	+0.427	This work
PAW/GGA	15 (S)		0.355	4.047	+1.166	+0.176	+0.856	This work
PAW/LDA	13 (AS)	0.410	0.409	4.179	+0.524	−0.560	+0.464	This work
PAW/LDA	13 (S)		0.428	4.174	+0.491	−0.528	+0.427	This work
PAW/LDA	15 (S)	0.429	0.427	4.179	+1.165	+0.176	+0.856	This work
Ps/GGA	6 (S)		0.357	4.18	+1.08	−0.10	+0.05	[44]
Ps/GGA	6 (S)			4.085	+1.06	−1.53	−0.54	[65]
AE/GGA	7 (S)		0.33	4.04	+1.35	+0.54	+1.06	[49]
AE/GGA	15 (S)	0.364	0.365	4.06	+1.15	−0.05	+0.46	[45]
AE/LDA	7 (S)		0.39	4.21	+1.35	+0.54	+1.04	[49]
AE/LDA	4 (S)		0.56	4.54				[66]
Exp.			0.50–0.52					[67]
Exp.			0.51	4.24				[68]
Exp.				4.48				[69]
LEED(300 K)					+2.2 ± 1.3			[70]
LEED(300 K)					+0.9 ± 0.5			[71]
LEED(300 K)					+1.8 ± 0.3	+0.1 ± 0.7		[72]
LEED(160 K)					+1.7 ± 0.3	+0.5 ± 0.7		[72]
LEED(300 K)					+1.3 ± 0.8			[73]

energies of the asymmetric slab with the number of layers n and the bulk total energy E_b:

$$E_{urlx}(n) = 2\sigma_{urlx} - nE_b \quad (5)$$

$$E_{rlx}(n) = \sigma + \sigma_{urlx} - nE_b \quad (6)$$

Among the different existing methods [45,49,53–60] of calculation of the surface energy in the slab geometry, this method is one of the most accurate one with a reduced number of layers [53,55–60].

The geometry of the slab (number of fixed, free layers and vacuum) was carefully optimized in order to obtain an accurate representation of the free Al surface with a reduced number of Al layers. A rigid slab of 3 Al layers was used to determine the size of the vacuum region: the number of vacuum layers n_v was increased until convergence of the unrelaxed surface energy of the Al slab within 0.01 meV/at. An asymmetric slab with a fixed number of 2 free Al layers was then used to fix the number n_r of Al rigid bulk layers: n_r was increased until convergence of both, the interlayer distance d of the free layers ($\delta d/d < 0.1\%$), and the applied forces on the last rigid layer (<0.05 eV/Å). Finally, the number n_f of free layers in the Al slab was increased until convergence of both, the asymmetric surface energy and the interlayer distance between the last rigid layer and first free layer ($\delta d/d < 10^{-4}\%$).

We thus chose a 13-layer slab geometry ($n_r/n_f/n_v = 6/7/5$, ≈14.1 Å vacuum) for the (111) surface. However, for the study of GP-zone segregation, we used a less converged geometry $n = 7$ ($n_b/n_f/n_v = 3/4/5$) in order to extend the surface to avoid interactions between the (100) GP clusters. In the case of the (100) surface we chose an 18-layer slab geometry ($n_r/n_f/n_v = 8/10/6$).

The work function Φ, is one of the most fundamental properties of a metallic surface. It is the minimum energy required to remove an electron from the surface. As such, it is of interest to a wide range of surface phenomena [61–64]. In particular, the measurement of work function changes $\Delta\Phi$, is routinely used in the study of adsorption processes on metal surfaces and photoemission. The work function is given by

$$\Phi = V_{es}(\infty) - E_F \quad (7)$$

where E_F is the Fermi energy of the system and $V_{es}(\infty)$ is the electrostatic potential at an infinite distance from the surface, evaluated in our calculations at the middle of the vacuum region of the slab.[2]

In order to test the accuracy of our representation of the (111) and (100) Al surfaces, we calculated the surface energy, work function and interlayer relaxations ($\Delta_{ij} = (d_{ij} - d_0)/d_0$ between the relaxed atomic layers i and $xtitj$ with respect to the bulk interlayer spacing d_0, with $i,j = 1,2,...$ from the surface layer down to the bulk). The calculations were performed with a one atom per surface unit cell supercell geometry and a $(15 \times 15 \times 1)$ k-point grid. Some test calculations have also been performed with a symmetric (S) configuration for comparison. The results are reported in Tables 4 and 5 together with known experimental values and previously published results. All other obtained results summarized in Tables 4 and 5 were calculated with a (S) configuration.

Our test calculations, with (S) configurations with the same or similar number of layers than the (AS) configurations, led to close values for the surface energy with both LDA and GGA XC functionals (to within 1 meV for the (100) surface and 20 meV for the (111) surface). The small discrepancies between our results and the two other pseudopotential studies [44,65] might be due to the small number of layers used in their study. Compared to all electron calculations, our pseudopotential calculations underestimate the surface energy by 19 meV with GGA and overestimate it by 31 meV with LDA. These differences are of the order of 5% only. Another important point is the very small relaxation energy of the surfaces, less than 2 meV. Our work function values agree, to within 1%, with those of the all electron calculations on (S) configurations with comparable number of layers. Concerning the surface interlayer relaxation there is a much wider dispersion. It is an expected result, since it is now well established [45,49,56] that Al surfaces are very sensitive to quantum size effects, [77–81] leading to long range interlayer oscillating relaxations and consequently a high sensitivity to the number of layers and the type of slab, (S) or (AS). Both the (AS) calculations and the pseudopotential calculations led to slightly erroneous values compared to the (S) and all electron calculations. However, this is not a critical issue for our study since the relaxations are small (this explains, also, why the relaxation energies are small).

All the preceding conclusions allow us to be confident in the accuracy of our forthcoming study of surface AlCu alloying and Cu segregation: the surface relaxations (distances and energy) are very

[2] In our slab geometry, the electrostatic potential is perfectly flat around the middle of the vacuum region. Thus, the electrostatic potential at the middle of the vacuum region equals the electrostatic potential at infinity.

Table 5
Calculated properties of the (100) Al surface and comparison to other calculations and known experimental values. Calculations (Ps: pseudo, AE: all electron) and number of layers n (S, AS: symmetric or asymmetric slab).Calculations and experiment (LEED = Low Energy Electron Diffraction): σ_{urlx}(eV/at.) unrelaxed and σ(eV/at.) relaxed surface energy, Φ(eV) work function and Δ_{ij}(%) relative interlayer distances (see text).

	n	σ_{urlx}	σ	Φ	Δ_{12}	Δ_{23}	Δ_{34}	Ref.
PAW/GGA	18 (AS)	0.430	0.432	4.265	+0.899	+0.243	+0.195	This work
PAW/GGA	19 (S)	0.433	0.431	4.251	+1.045	+0.177	+0.526	This work
PAW/LDA	18 (AS)	0.501	0.499	4.427	+0.829	+0.218	+0.250	This work
PAW/LDA	19 (S)		0.499	4.417	+0.892	+0.274	+0.532	This work
AE/GGA	17 (S)	0.486	0.484	4.243	+1.598	+0.436	−0.002	[45]
AE/GGA	4 (S)		0.689					[74]
AE/GGA	13 (S)				+0.5	−0.3		[75]
LEED(100 K)					+2.0±0.8%	+1.2±0.8		[76]

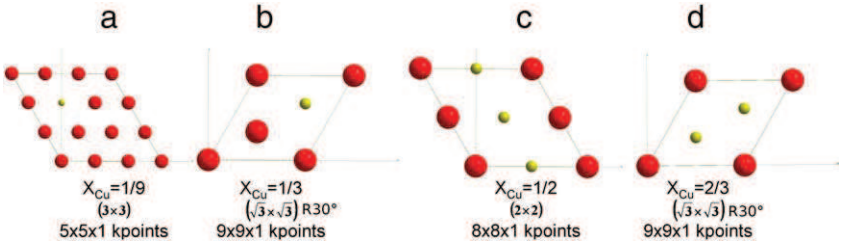

Fig. 2. The studied (111) Cu–Al layer configurations. Big balls represent Al atoms and small balls represent Cu atoms.

small and the absolute values calculated with the pseudopotential approach agree with all electron calculations within less than 5%. Thus, we expect that the alloying and segregation energies calculated with the pseudopotential approximation and our asymmetric slab configurations will be comparable to those of an all electron calculation, since these two configurations are not much different.[3]

4. Copper surface segregation

As discussed in the Introduction, it is experimentally [8–10] and theoretically [15,82,83] well established that increasing Cu concentration in the α phase of the Al–Cu phase diagram, results in Cu (100) clustering leading to the formation of the GP-zones [6,7] which are the precursors of the θ' and θ phases that stabilize at higher Cu concentration. Such Cu precipitation, if it happens at the Al surface, can change drastically its properties. Energetically, as we have seen, the most favorable surface for aluminum is the dense (111) surface. The next surface to be considered is the (100) surface whose energy is about 25% more energetic. The (111) surface is then highly representative of the surface of any bulk piece of aluminum. In the following we first present the results of the Cu surface segregation at the (111) Al surface as a function of Cu concentration and then those of the GP-zone segregation at both surfaces. For this study we used the LDA approximation since it usually gives, thanks to a compensation of errors between the exchange and correlation energies, more accurate results than the GGA approximation [52,84,85]. However, in some cases we also performed GGA calculations for comparison. We made a layer by layer surface segregation study: an increasing number of Al atoms are substituted by Cu atoms in a given Al layer l ($l=1,2,3,...$ from the surface down to the bulk), parallel to the (111) surface. The Cu–Al layer position is then varied from the surface down to the bulk. The Cu concentration c_l in layer l, has been varied from the almost dilute limit 1/9 (see Section 3.1) up to a complete Cu monolayer for the consideration of Cu clustering and ordering effects at the surface. The same procedure has been applied for the study of GP-zone surface segregation with a full Cu monolayer for the (100) surface. For the (111) surface we could only consider very small (100) clusters due to the limited thickness of the slab. The segregation energy per Cu atom, with Cu layer concentration c_l in surface layer l, is defined as the energy gained, per Cu atom, by the $Al_{1-x}Cu_x$ alloy when a concentration c_l of Cu atoms are transferred from a bulk layer to that of the surface layer:

$$E_{seg}(c_l) = \frac{E(c_l,x) - lim_{l\to\infty}E(c_l,x)}{c_l} \tag{8}$$

where $E(c_l,x)$ is the energy of a semi-infinite $Al_{1-x}Cu_x$ alloy with a c_l Cu concentration in layer l. When l tends to infinity, $E_{seg}(c_l)$ tends to zero.

4.1. Cu surface segregation in (111) Al

The studied Cu–Al layer configurations are reported on Fig. 2. With the adopted slab geometry ($n_r/n_f/n_v = 6/7/5$) Cu atoms could be buried only up to the fourth layer without any interaction with the fixed layers.

4.1.1. Al(111) Cu segregation in the single atom limit

At the lowest Cu concentration (Fig. 2(a)), $c_l = 1/9 = 0.11\%$, Cu atoms can be considered as independent (Section 3.1). In this dilute limit and in the slab geometry, with N atoms per layer and N_l Cu atoms in layer l, the segregation energy per Cu atom is evaluated by:

$$E_{seg}\left(\frac{N_l}{N}\right) = \frac{E_{slab}(N_l) - E_{slab}(0)}{N_l} + E_c(Al) - \mu_{Cu}(x\to 0) \tag{9}$$

where $E_{slab}(N_l)$ is the energy of the slab with N_l Cu atoms in layer l and $\mu_{Cu}(x\to 0)$ the Cu chemical potential in the $Al_{1-x}Cu_x$ dilute alloy (Eq. 4).

The evolution of the segregation energy with the layer position l is reported on Fig. 3 (full line). Clearly, the surface position is a highly unfavorable position with high positive segregation energy. The sub-surface and sub-sub-surface positions are more stable ($E_{seg}<0$) than

[3] It is generally admitted and sustained by today's long experience of DFT calculations, that inaccuracies in DFT calculations, due to unavoidable approximations, are rather systematic and cancelled when computing energy differences between configurations which are not too much different, as far as they contain the same number of atoms of each species of course.

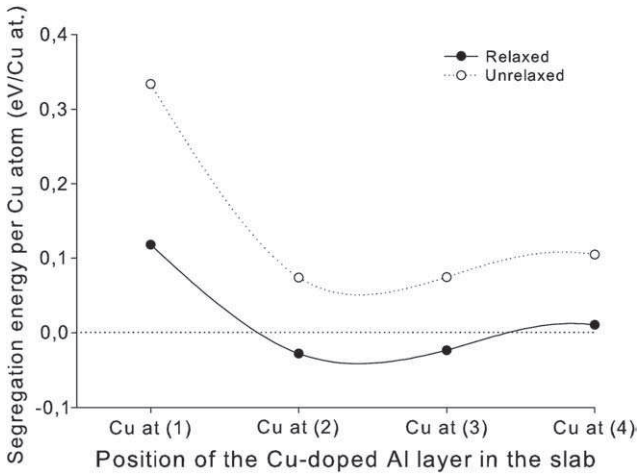

Fig. 3. Cu-(111)Al surface segregation energy at infinite dilution ($C_l = 0.11\%$) versus depth l, Cu(l): dashed line before atomic relaxation, full line after atomic relaxation.

the bulk one, whereas the $l = 4$ layer position can be assimilated to the bulk one within the uncertainty of the calculation. The sub-surface position appears as the most stable one with a rather low segregation energy (of the order of −30 meV), a value nevertheless significant compared to the uncertainty due to the oscillations of the surface energy due to quantum size effects which are of the order of 5–10 meV [45].

In the dilute limit, the surface segregation energy is usually decomposed into three independent contributions corresponding to three thermodynamic forces: [86–88]

- The surface force which is proportional to the surface energy difference between the two pure metals. This force favors the segregation at the surface of the element with the lowest surface energy, which, in our case, is aluminum ($\sigma_{Cu} = 0.640$ eV/at. [49] compared to $\sigma_{Al} = 0.409$ eV/at.).
- The ordering or mixing force, proportional to the mixing energy which favors surface segregation when positive (tendency to demixion). Here also this force will favor Al at the surface since the segregation energy is negative (Section 3.1).
- The elastic energy force proportional to the difference in elastic strain energy between the layer and the bulk which is due to the solute–solvent atomic size mismatch. In the dilute limit, it always favors the segregation of the solute atoms at the surface, hence the Cu surface segregation in our case.

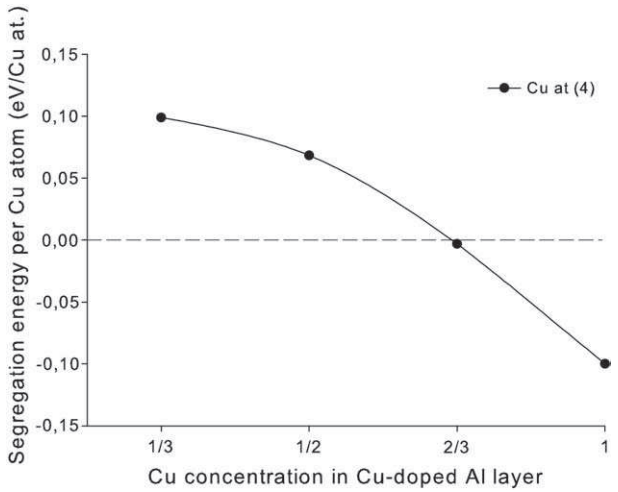

Fig. 4. Cu Segregation energy at (111)Al surface versus Cu concentration in layer (4).

In agreement with this model, the unrelaxed segregation energies (dashed curve on Fig. 3) are positive and lead to a rapidly decreasing segregation energy with depth. Interestingly, in this unrelaxed picture and considering that the bulk unrelaxed value has been reached at $l = 4$, the sub- and sub-sub-surface positions are much stable than the bulk one, in contradiction with the previous model which appears then has been valid only for the surface layer. A much complex description of the surface segregation energy, taking into account the evolution and the interaction of these forces with the solute layer position, is then necessary for a proper description of the undersurface layer by layer segregation [89]. The effect of the third thermodynamic force, even if it is an important effect does not change the previous picture. Even if it is much more pronounced at the surface layer, it is not sufficient in that case to overcompensate the effect of the two other forces which are much larger at the surface layer and its main effect is to increase slightly the stability of the subsurface and sub-sub-surface positions. Finally, the Cu segregation at the sub- and sub-sub-surface layers results mainly from a complex interaction between the surface and mixing forces which individually are not favorable to such a Cu segregation.

4.1.2. Alloying and ordering effects

In this part, the Cu concentration in a given layer is increased up to 1 (full Cu monolayer). With the limited surface size of the simulation

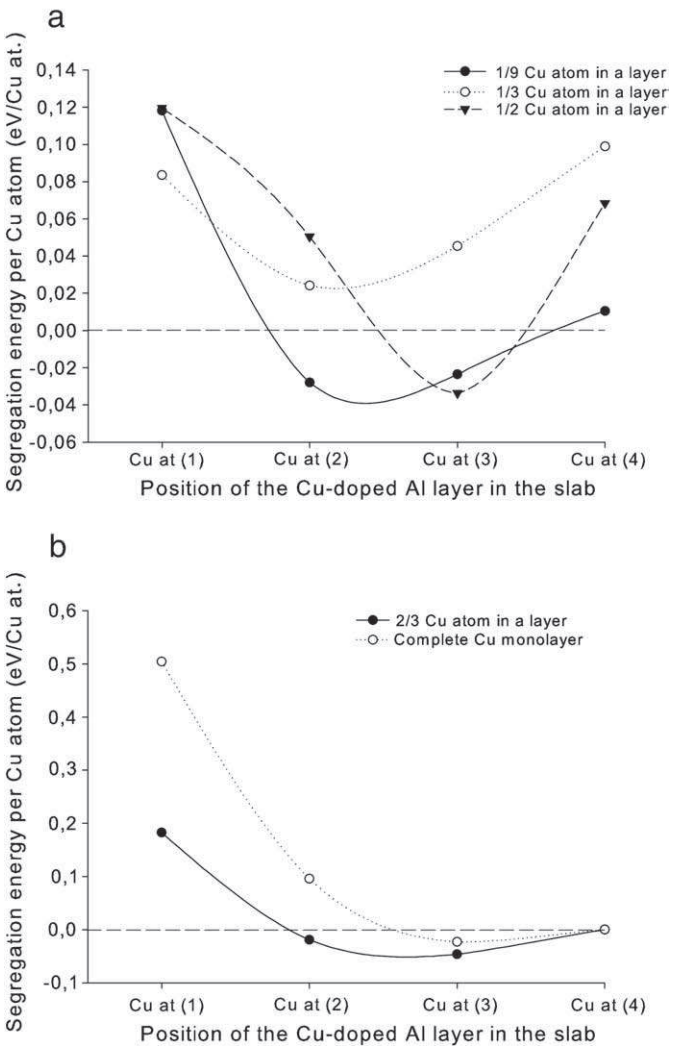

Fig. 5. Cu segregation energy at (111) Al surface versus layer position (l) for different Cu concentrations, c_l. (a): $c_l \leq 1/2$, deduced from Eq. (9). (b): $c_l > 1/2$, deduced from Eq. (10).

cell, the studied intermediate concentrations (1/3, 1/2 and 2/3) correspond to different ordered layer structures shown in Fig. 2(b), (c) and (d). In these configurations, the Cu atoms interact and the reference state for defining the segregation energy depends on the tendency or not to clustering in the bulk. In the absence of a clustering tendency in the bulk (positive interaction energy), the reference state remains the one used in Eq. (9), but if there is a tendency to clustering, the reference bulk state must be the clustered configuration. In that case the segregation energy can be evaluated by:

$$E_{seg}\left(\frac{N_l}{N}\right) = \frac{E_{slab}(N_l) - E_{slab}\left(N_{l_b}\right)}{N_l} \tag{10}$$

where l_b is large enough for $E_{slab}(N_{l_b})$ to be converged to the bulk value. From what we have seen in the dilute Cu limit the bulk configuration is almost reached at layer (4). So we will make the approximation that this is also the case at any Cu concentration for the evaluation of the bulk configuration energy. Fig. 4 reports the evolution of E_{seg}, deduced from Eq. (9), with Cu concentration in layer (4). It shows that, in this approximated bulk limit, there is a strong interaction between the Cu atoms in a given (111) plane. This interaction corresponds to a tendency to Cu clustering only for the layer structures with high Cu concentrations: 2/3 and the full Cu monolayer. This is not in contradiction with the experimentally observed tendency to Cu GP-zone clustering in the α-AlCu phase, since this clustering occurs in (100) planes.

Thus, the segregation energies for the configurations with Cu concentrations lower or equal to 1/2 have been calculated with Eq. (9) and are reported on Fig. 5(a), whereas for higher Cu concentrations they are calculated with Eq. (10) with $l_b = 4$ and reported on Fig. 5(b).

At high concentrations (1 and 2/3: Fig. 5(b)) there is always a surface segregation in the sub-sub-surface layer (3). For the 1/2 concentration (linear <110> structure), contrary to the bulk, clustering is favored with a negative segregation energy in the sub-sub-surface position. <110> directions belong to both the (111) and (100) plane families, thus this specific layer configuration can be viewed as a local linear GP-zone in a (111) plane whose structure is then stabilized by the surface in the sub-sub-surface layer. Finally, for the 1/3 Cu concentration ($(\sqrt{3}x\sqrt{3})R30^\circ$ structure), like for the bulk, clustering is not favored with positive segregation energies at all layer positions.

The strong Cu–Cu interactions induce also quite strong relaxations. As an example we show in Fig. 6 the outplane and inplane relaxations for the $c_l = 2/3$ case in the surface, sub-surface, and sub-sub-surface layers. In the vertical direction we observe a strong contraction of the distances between the alloy layer and the neighboring Al layers. For the surface and the sub-surface layer configurations, the Cu atoms relax inwards respectively by 0.32 Å and 0.06 Å relative to the Al neighbors in the same layer. For the sub-sub-surface configuration, the Cu atoms relax slightly outward by 0.03 Å. Within the alloy layer, the distances between the Cu atoms and their nearest neighbors contract and the distances between the nearest and next-nearest neighbors (which are nearest neighbors to another Cu impurity) expand by about the same amount (≈0.10 Å). Similarly, Cu–Al distances to nearest neighbors in another layer contract. Independently of the concentration, when Cu atoms are located on layer (2) or layer (3), there is a very strong contraction of the distance between the Cu atoms and their nearest-neighbors Al atoms located in the above layer. For all configurations, with decreasing Cu concentration, the interlayer distance between the alloy layer and its neighbors increases. Similar results have been obtained using GGA functional. This geometric distortions of the crystal around Cu clusters are very similar to the one observed around the GP-zones.

Finally, there is a tendency to segregation in the sub- and/or sub-sub-surface layers with strong relaxation effects.

4.2. GP-zone segregation

4.2.1. (111) surface

Since it appears that there is a tendency to segregation in both the sub-surface and the sub-sub-surface layers, one can expect a multilayer segregation with an increased stability compared to single layer segregation. Cu is known to form GP-zones, thus this multilayer segregation will develop in the form of small GP-zones. We model this multilayer GP-zone segregation with small clusters of 3 Cu atoms in a

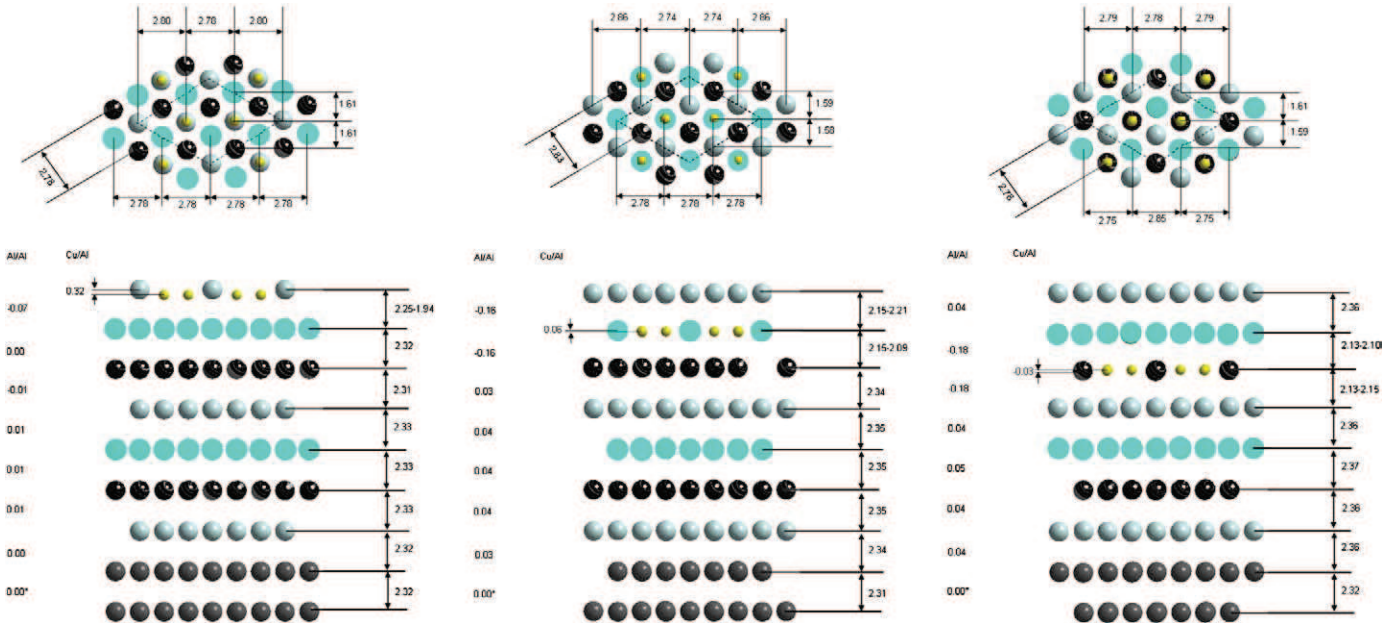

Fig. 6. Geometry of the relaxed $\left(\sqrt{3} \times \sqrt{3}\right)R30^\circ$ surface alloys with a layer coverage of $x_{Cu} = 2/3$, when the Cu impurities are in the top surface layer (1) (left), in sub-surface layer (2) (middle), and in layer (3) (right). Results obtained using LDA functional. All distances are in Å. The distances indicated on the left side of each slab correspond to the buckling of the layer. An asterisk denotes fixed layers. Large (small) balls representAl (Cu) atoms. Grey, light green and black atoms are located in the first (1), second (2), and third (3) layers, respectively.

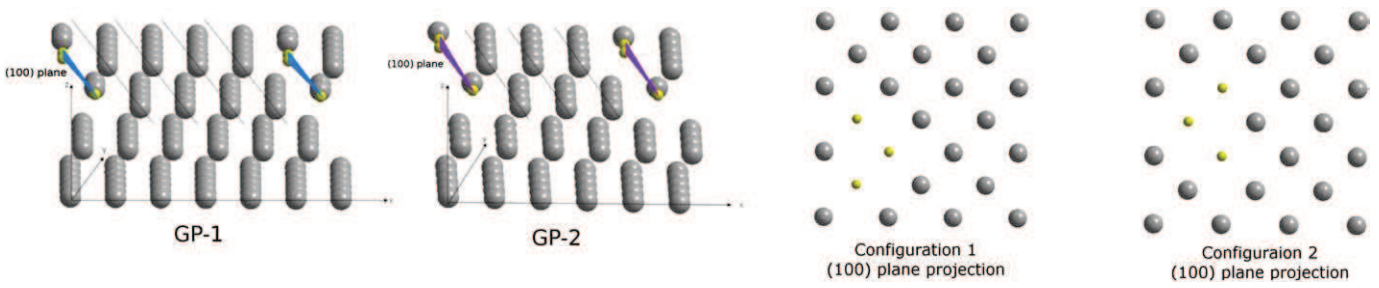

Fig. 7. Big balls: Al atoms. Small balls: Cu atoms. Cu atoms are in the (100) plane. Full lines represent the (100) Al planes between each Cu cluster and its periodic image in the slab. Configuration-1 represents the Cu (100) cluster such as 2 Cu atoms are closer to the surface and the third Cu atom is buried one layer beneath them. Configuration-2 represents the Cu (100) cluster such as 1 Cu atom is closer to the surface and the 2 other Cu atoms are buried one layer beneath it.

(100) plane. For the GP1 zones, the Cu clusters are separated by 4 (100) Al planes in order to avoid interactions between the clusters (GP-1 — Fig. 7). With this geometry, there are 25 atoms/layer. For the GP2 zones, the Cu clusters are separated by three Al(100) layers in the Al matrix (GP-2 — Fig. 7), corresponding to 16 atoms/layer. For both clusters, two configurations were considered: configuration-1, with 2 Cu atoms close to the surface and the third Cu atom beneath them, and configuration-2, symmetric of configuration one with 1 Cu atom close to the surface and the 2 other Cu atoms beneath it (Fig. 7). The clusters in both configurations were then buried in the slab in order to study the influence of the surface. These calculations were performed in both the LDA and the GGA approximations. As previously stated, for these calculations we had to use thinner slabs to keep reasonable computational time (7 layer slab: $n_r/n_f/n_v = 4/3/5$ corresponding respectively to 175 atoms and 112 atoms for the GP1 and GP2 clusters). The surface energy calculated with this slab is 4.00 meV/at. higher than the one calculated with the 13 layers slab, using both LDA and GGA functionals.

Table 6 shows the results of GP1-zones and GP2-zones segregation energies per Cu atom deduced from Eq. (9) as a function of their depth in the slab relative to the surface. These results show clearly that for both clusters and configurations (1 or 2), the system is much stable when the clusters are buried one layer under the surface, corresponding to a multilayer segregation in the sub- and sub-sub-surface layers. The segregation energies per Cu atom are larger in the LDA approximation than in the GGA approximation and the Cluster-1 configuration is much stable than the Cluster-2 configuration, no matter the cluster depth in the slab reflecting the higher stability of GP1-zones relative to GP2-zones [15]. In the LDA approximation, compared to the single atom segregation limit, the segregation energies per Cu atom are of the order of −300 meV/at. To compare with, we also calculated the segregation energy per Cu atom for the dilute impurities (taken as $x_C^u = 1/9$) using a 7-layers slab (Fig. 8). The segregation energy per Cu atom for the GP1-zones is 450 meV/at. lower than for dilute impurities, reflecting the very strong clustering tendency of Cu into GP1 zones. Compared to the same cluster in the bulk, taken here as position 3, the segregation energy per Cu atom of position 2 is of the order of 80 meV/at. more stable. It is larger than for dilute impurities where the sub-surface position is 50 meV/at. more stable than the position 3 (Fig. 8).

To conclude, there is a strong tendency to Cu segregation just below the surface layer of the (111) Al surface, in the form of GP1-zones and a less marked tendency in the form of GP2-zones.

4.2.2. (100) surface

Since the GP-zones are Cu platelets in (100) Al planes and, the (100) Al surface is the second most common surface of aluminum, it is important to see if there is a tendency to segregation of the GP-zones at the (100) Al surface. We thus studied the segregation of a full Cu monolayer in a (100) Al slab ($n_r/n_f/n_v = 8/10/6$). In this case, a simple way to check the convergence of Eq. (10) to the bulk configuration, is to use the substitution energy of an Al monolayer (ML) by a Cu ML at different depth l, defined by:

$$E_{\text{sub}}(l) = E_{\text{tot}}^{\text{slab}}(l) - \left(E_{\text{Al}}^{\text{surf}} + E_{\text{Cu}}^{\text{ML}}\right) \tag{11}$$

where $E_{\text{tot}}^{\text{slab}}(l)$ is the total energy of the (100) Al slab with a Cu monolayer (ML) in layer l, $E_{\text{Al}}^{\text{surf}}$ the total energy of the pure (100) Al slab and $E_{\text{Cu}}^{\text{ML}}$ the free-standing Cu ML energy with in plane lattice constant equal to that of the Al lattice ($d_{\text{Cu-Cu}}^{\text{LDA}} = 2.79$ Å and $d_{\text{Cu-Cu}}^{\text{GGA}} = 2.83$ Å). For $l \to \infty$ this substitution energy converges towards the substitution energy in the bulk E_{sub}^b:

$$E_{\text{sub}}^b = E_{\text{tot}}^b - \left(E_{\text{Al}} + E_{\text{Cu}}^{\text{ML}}\right) \tag{12}$$

where E_{tot}^b is the energy of an Al crystal with a Cu ML and E_{Al} the energy of this same Al perfect crystal.

Table 6
Segregation energies for GP-zone clusters segregation at (111)Al surface. GP1 zone, GP2 zone. Pos 1: cluster in layers (1–2). Pos 2: clusters in layers (2–3). Pos 3: clusters in layers (3–4). Conf-1: 2 Cu atoms in the upper layer. Conf-2: 1 Cu atom in the upper layer.

		Segregation energy (eV/at.)					
		Pos 1		Pos 2		Pos 3	
		LDA	GGA	LDA	GGA	LDA	GGA
Conf. 1	GP-1	−0.263	−0.089	−0.312	−0.117	−0.232	−0.047
	GP-2	−0.124	0.025	−0.160	0.009	−0.105	0.058
Conf. 2	GP-1	−0.196	−0.104	−0.201	−0.100	−0.108	−0.018
	GP-2	−0.086	0.014	−0.093	0.017	−0.020	0.081

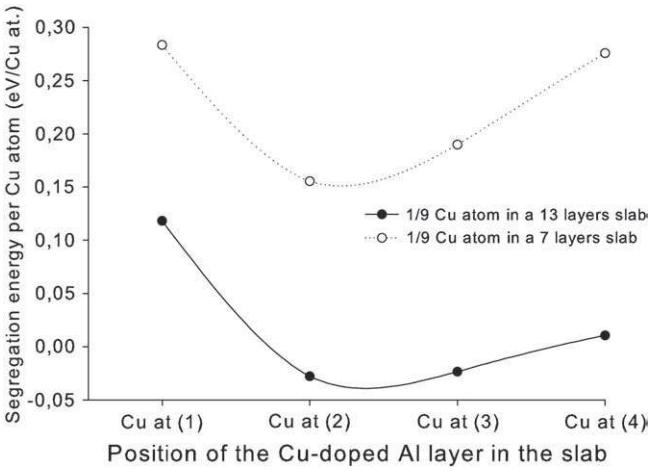

Fig. 8. Cu-(111)Al surface segregation energy at infinite dilution ($C_l = 0.11\%$) versus depth l, Cu(l): dashed line in a 7 layers slab, full line in a 13 layers slab.

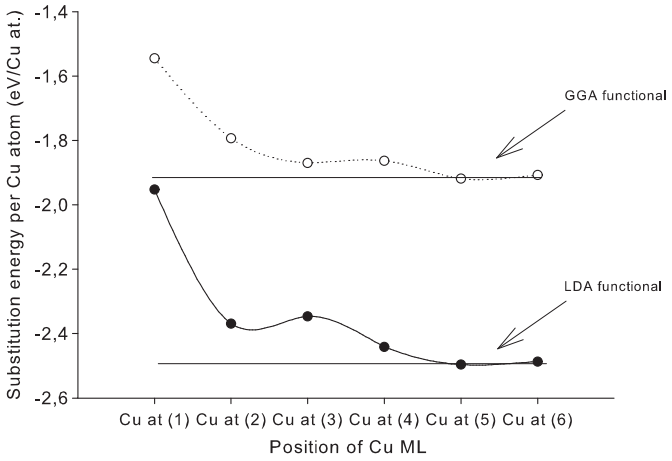

Fig. 9. Substitution energy of the (100)Cu monolayer for different positions within the slab. Calculations are done using both LDA and GGA functionals. Dashed lines are the substitution energies of Cu monolayers within the bulk.

The evolution of the substitution energy of the Cu (100) monolayer for different depth l relative to the surface is reported in Fig. 9 in both the LDA and GGA approximations, together with the bulk substitution energy. As one can see, in both cases, at $l=6$, $E_{sub}(l=6)$ equals the bulk substitution energy E^b_{sub}. More importantly, the segregation energy (difference between surface and bulk substitution energies) is always positive. Thus, there is no tendency to surface segregation of GP-zones at the (100) Al surface. There is even a barrier to segregation at $l=3$ in the LDA and $l=4$ in the GGA approximations.

5. Conclusion

In this paper we present a detailed density functional theory slab calculations for various configurations of Cu atoms in Al-rich matrix. We studied Cu infinite dilution in bulk, surface alloys properties for varying compositions of Cu-doped layers as well as first stage formation of Guinier–Preston zones, in the surface and then buried in an Al slab.

To investigate the Al–Cu interactions in bulk phase at low Cu concentrations, we chose three different Cu atomic concentrations ($x=0.92\%$, 1.52% and 3.12%). We got weak negative values of the mixing enthalpies, that indicate a low tendency to the formation of a solid solution in the absence of any competing ordered phase at $T=0$ K.

The asymmetric configuration used to build the slabs modeling the (111) and (100) surfaces, enables the use of thicker slabs and a low number of relaxed layers by considering only one free surface on one side of the slab. The study of Cu doped (111) layers in an Al-rich matrix, showed that within a given layer, the energy of formation shows a strong dependence on its composition and its position in the slab. Thus, in the absence of ordering effects for Cu atoms in a layer ($x_{Cu}=1/9$ and $x_{Cu}=1/3$), the system is more stable when the doped layer is buried one layer under the surface (2), whereas for $x_{Cu}=1/2$ to $x_{Cu}=1$ (full monolayer), the doped layer is more accommodated when buried two layers under the surface (3). However, for all Cu concentrations in a layer, the surface position is highly unstable. Taking as the reference state for the segregation energy the tendency or not to clustering in the bulk, we find that at low Cu concentration ($x_{Cu}\leq 1/2$), Cu atoms do not form clusters in the bulk, whereas at high Cu concentrations ($x_{Cu}=2/3$ and $x_{Cu}=1$), this tendency is strong, in good agreement with the Al–Cu phase diagram, predicting the Cu clustering in the α-Al–Cu phase.

Modeling first stages formation of GP-1 and GP-2 zones by doping (100)Al layers with Cu clusters in a (111)Al slab, in the surface then buried one and two layers under the surface, resulted in segregation energies favoring Cu clusters buried close to the surface. For all positions in the slab, GP-1 is more stable than GP-2, which is in good agreement with experimental observations. The stability of these multilayer clusters is in good agreement with Al–Cu solid transformation which predicts, at room temperature and small Cu concentration, the occurrence of the first stable precipitates by the formation of GP1 zones. It also confirms and fits with tendency for Cu-doped single layers to segregate in the sub-surface and sub-sub-surface.

However the segregation of a full copper (100) monolayer in an (100)Al matrix shows a copper segregation deep in the bulk with even, for both used XC functionals, a segregation barrier.

The segregation of Cu atoms is observed in the (111) Al matrix close to the surface rather than in the bulk, suggesting overall a strong interaction between the surface and the Cu atoms. Therefore, it will be interesting to investigate Cu segregation behavior when adsorbing on the surface atoms, molecules or small clusters.

Acknowledgments

The authors are grateful to Dr Hao Tang for very stimulating discussions. This work has been supported by the National Research Agency ASURE (ANR support number BLAN08-2_342506) and by the French ministry of research. This work was granted access to the HCP resources of CINES under allocation 2009_095076 made by GENCI (Grand Equipement National de Calcul intensif), and to the HCP resources of CalMiP (Calcul Midi-Pyrenees) under project number P0840.

References

[1] W. Zhou, L. Liu, B. Li, Q. Song, P. Wu, J. Electron. Mater. 38 (2) (2009) 356.
[2] C. Hang, C. Wang, M. Mayer, Y. Tian, Y. Zhou, H. Wang, Microelectron. Reliab. 48 (3) (2008) 416, doi:10.1016/j.microrel.2007.06.008.
[3] T. Hoshino, N. Fujima, M. Asato, R. Tamura, J. All. Comp. 434–435 (2007) 572.
[4] J. Korringa, Physica 13 (1947) 392.
[5] W. Kohn, N. Rostoker, Phys. Rev. 94 (5) (1954) 1111, doi:10.1103/PhysRev.94.1111.
[6] A. Guinier, Nature 142 (1938) 569.
[7] G.D. Preston, Nature 142 (1938) 570.
[8] V. Gerold, Z. Metall. 45 (1954) 599.
[9] A. Guinier, Solid State Phys. 9 (1959) 293.
[10] V. Gerold, Scr. Metall. 22 (7) (1988) 927.
[11] J.B. Cohen, Solid State Phys. 39 (1986) 131.
[12] T.J. Konno, K. Hiraga, M. Kawasaki, Scr. Mater. 44 (8–9) (2001) 2303.
[13] M.J.G. Lee, M. Gensch, A.I. Shkrebtii, T. Herrmann, W. Richter, N. Esser, P. Hofmann, Phys. Rev. B 72 (2005) 085408.
[14] M. Braunovic, N. Alexandrov, Components, Packaging, and Manufacturing Technology, Part A, IEEE Transactions on, 17 (1), 1994, p. 78.
[15] S. Wang, M. Schneider, H. Ye, G. Gottstein, Scr. Mater. 51 (7) (2004) 665.
[16] V. Vaithyanathan, C. Wolverton, L.Q. Chen, Phys. Rev. Lett. 88 (12) (2002) 125503, doi:10.1103/PhysRevLett.88.125503.
[17] V. Vaithyanathan, C. Wolverton, L. Chen, Acta Mater. 52 (2004) 2973.
[18] C. Wolverton, V. Ozolins, Phys. Rev. Lett. 86 (2001) 5518.
[19] C. Wolverton, V. Ozolins, Phys. Rev. B 73 (2006), 144104–1–14.
[20] C. Wolverton, V. Ozolins, A. Zunger, J. Phys. Condens. Matter 12 (2000) 2749.
[21] C. Wolverton, X.-Y. Yan, R. Vijayaraghavan, V. Ozolins, Acta Mater. 50 (2002) 2187.
[22] P. Hohenberg, W. Kohn, Phys. Rev. 136 (3B) (1964) B864.
[23] W. Kohn, L.J. Sham, Phys. Rev. 140 (4A) (1965) A1133, doi:10.1103/PhysRev.140.A1133.
[24] P. Goodman, Fifty years of electron diffraction, Reidel, 1981.
[25] G. Binnig, N. Garcia, H. Rohrer, J.M. Soler, F. Flores, Phys. Rev. B 30 (8) (1984) 4816.
[26] B.N.J. Persson, A. Baratoff, Phys. Rev. B 38 (14) (1988) 9616.
[27] A.A. Lucas, H. Morawitz, G.R. Henry, J.-P. Vigneron, P. Lambin, P.H. Cutler, T.E. Feuchtwang, Phys. Rev. B 37 (18) (1988) 10708, doi:10.1103/PhysRevB.37.10708.
[28] P.M. Echenique, A. Gras-Marti, J.R. Manson, R.H. Ritchie, Phys. Rev. B 35 (14) (1987) 7357, doi:10.1103/PhysRevB.35.7357.
[29] G. Doyen, E. Koetler, J.-P. Vigneron, M. Scheffler, Appl. Phys. A Solids Surf. 51 (1990) 281.
[30] G. Kresse, J. Hafner, Phys. Rev. B 47 (1) (1993) 558, doi:10.1103/PhysRevB.47.558.
[31] G. Kresse, J. Furthmüller, Phys. Rev. B 54 (16) (1996) 11169, doi:10.1103/PhysRevB.54.11169.
[32] G. Kresse, J. Furthmüller, Comput. Mater. Sci. 6 (1) (1996) 15, doi:10.1016/0927-0256(96)00008-0.
[33] P.E. Blöchl, Phys. Rev. B 50 (24) (1994) 17953.
[34] G. Kresse, D. Joubert, Phys. Rev. B 59 (3) (1999) 1758, doi:10.1103/PhysRevB.59.1758.
[35] D.M. Ceperley, B.J. Alder, Phys. Rev. Lett. 45 (7) (1980) 566.
[36] J.P. Perdew, J.A. Chevary, S.H. Vosko, K.A. Jackson, M.R. Pederson, D.J. Singh, C. Fiolhais, Phys. Rev. B 46 (11) (1992) 6671, doi:10.1103/PhysRevB.46.6671.

[37] J.P. Perdew, A. Zunger, Phys. Rev. B 23 (10) (1981) 5048, doi:10.1103/PhysRevB.23.5048.
[38] J.P. Perdew, K. Burke, M. Ernzerhof, Phys. Rev. Lett. 77 (18) (1996) 3865, doi:10.1103/PhysRevLett.77.3865.
[39] M. Methfessel, A.T. Paxton, Phys. Rev. B 40 (6) (1989) 3616, doi:10.1103/PhysRevB.40.3616.
[40] H.J. Monkhorst, J.D. Pack, Phys. Rev. B 13 (12) (1976) 5188, doi:10.1103/PhysRevB.13.5188.
[41] P. Pulay, Chem. Phys. Lett. 73 (2) (1980) 393, doi:10.1016/0009-2614(80)80396-4.
[42] C. Kittel, Introduction to Solid State Physics, 6th EditionWiley, New York, 1986.
[43] A. Khein, D.J. Singh, C.J. Umrigar, Phys. Rev. B 51 (7) (1995) 4105, doi:10.1103/PhysRevB.51.4105.
[44] Y. Yourdshahyan, B. Razaznejad, B.I. Lundqvist, Phys. Rev. B 65 (2002), 075416–1–17.
[45] J.L.F. Da Silva, Phys. Rev. B 71 (19) (2005) 195416, doi:10.1103/PhysRevB.71.195416.
[46] M. Fuchs, J.L.F. Da Silva, C. Stampfl, J. Neugebauer, M. Scheffler, Phys. Rev. B 65 (24) (2002) 245212.
[47] M. Fuchs, M. Bockstedte, E. Pehlke, M. Scheffler, Phys. Rev. B 57 (4) (1998) 2134, doi:10.1103/PhysRevB.57.2134.
[48] C. Domain, C.S. Becquart, Phys. Rev. B 65 (2) (2001) 024103.
[49] J.L.D. Silva, C. Stampfl, M. Scheffler, Surf. Sci. 600 (3) (2006) 703, doi:10.1016/j.susc.2005.12.008.
[50] F.D. Murnaghan, Proc. Natl Acad. Sci. USA 50 (1944) 697.
[51] J.P. Perdew, K. Burke, Int. J. Quantum Chem. 57 (1996) 309.
[52] S. Kurth, J.P. Perdew, P. Blaha, Int. J. Quantum Chem. 75 (4–5) (1999) 889.
[53] J.G. Gay, J.R. Smith, R. Richter, F.J. Arlinghaus, R.H. Wagoner, J. Vacuum Sci. Technol. A Vacuum Surf. Films 2 (2) (1984) 931, doi:10.1116/1.572482.
[54] P.J. Feibelman, D. Hamann, Surf. Sci. 234 (3) (1990) 377, doi:10.1016/0039-6028(90)90570-X.
[55] J.C. Boettger, Phys. Rev. B 49 (23) (1994) 16798.
[56] J.C. Boettger, Phys. Rev. B 53 (19) (1996) 13133, doi:10.1103/PhysRevB.53.13133.
[57] V. Fiorentini, M. Methfessel, J. Phys. Condens. Matter 8 (36) (1996) 6525.
[58] P.J. Feibelman, Surf. Sci. 360 (1–3) (1996) 297, doi:10.1016/0039-6028(96)00599-7.
[59] V. Fiorentini, M. Methfessel, J. Phys. Condens. Matter 10 (4) (1998) 895.
[60] J.C. Boettger, J.R. Smith, U. Birkenheuer, N. Rösch, S.B. Trickey, J.R. Sabin, S.P. Apell, J. Phys. Condens. Matter 10 (4) (1998) 893.
[61] M.-C. Desjonquères, D. Spanjaard, Springer series in Surface Physics, 2nd Edition, Springer, 1996.
[62] J.B. Hudson, Surface Science: An introduction, John Wiley, 1998.
[63] C.J. Fall, N. Binggeli, A. Baldereschi, Phys. Rev. Lett. 88 (15) (2002) 156802.
[64] A. Michaelides, P. Hu, M.-H. Lee, A. Alavi, D.A. King, Phys. Rev. Lett. 90 (24) (2003) 246103.
[65] A. Kiejna, B.I. Lundqvist, Phys. Rev. B 63 (8) (2001) 085405, doi:10.1103/PhysRevB.63.085405.
[66] H.L. Skriver, N.M. Rosengaard, Phys. Rev. B 46 (11) (1992) 7157, doi:10.1103/PhysRevB.46.7157.
[67] W. Tyson, W. Miller, Surf. Sci. 62 (1) (1977) 267, doi:10.1016/0039-6028(77)90442-3.
[68] F.R. De Boer, R. Boom, W.C.M. Mattens, A.R. Miedema, A.K. Niessen, Vol.1 of Cohesion and structure, North-Holland, Amsterdam, 1989.
[69] Zeppenfeld, Physics of Covered Solid Surfaces, Landolt-Börnstein, New series, Group III, Vol. vol. 42: Numerical Data and functional Relationships in Science and Technology, Subvol. A: Adsorbed Layers on Surfaces, Springer-Verlag, Berlin, 2001, p. 67.
[70] F. Jona, D. Sondericker, P.M. Marcus, J. Phys. C: Solid State Phys. 13 (8) (1980) L155.
[71] H.B. Nielsen, D.L. Adams, J. Phys. C: Solid State Phys. 15 (3) (1982) 615.
[72] J.R. Noonan, H.L. Davis, J. Vacuum Sci. Technol. A Vacuum Surf. Films 8 (3) (1990) 2671.
[73] C. Stampfl, M. Scheffler, H. Over, J. Burchhardt, M. Nielsen, D.L. Adams, W. Moritz, Phys. Rev. B 49 (7) (1994) 4959.
[74] L. Vitos, A.V. Ruban, H.L. Skriver, J. Kollàr, Surf. Sci. 411 (1-2) (1998) 186, doi:10.1016/S0039-6028(98)00363-X.
[75] M. Borg, M. Birgersson, M. Smedh, A. Mikkelsen, D.L. Adams, R. Nyholm, C.-O. Almbladh, J.N. Andersen, Phys. Rev. B 69 (2004) 235418, doi:10.1103/PhysRevB.69.235418.
[76] J.H. Petersen, A. Mikkelsen, M.M. Nielsen, D.L. Adams, Phys. Rev. B 60 (8) (1999) 5963, doi:10.1103/PhysRevB.60.5963.
[77] R.C. Jaklevic, J. Lambe, M. Mikkor, W.C. Vassell, Phys. Rev. Lett. 26 (2) (1971) 88, doi:10.1103/PhysRevLett.26.88.
[78] R.C. Jaklevic, J. Lambe, Phys. Rev. B 12 (10) (1975) 4146, doi:10.1103/PhysRevB.12.4146.
[79] F. Schulte, Surf. Sci. 55 (2) (1976) 427.
[80] P.J. Feibelman, Phys. Rev. B 27 (4) (1983) 1991.
[81] I.P. Batra, S. Ciraci, G.P. Srivastava, J.S. Nelson, C.Y. Fong, Phys. Rev. B 34 (12) (1986) 8246, doi:10.1103/PhysRevB.34.8246.
[82] C. Wolverton, Phil. Mag. Lett. 79 (1999) 683.
[83] S. Muller, L.-W. Wang, A. Zunger, C. Wolverton, Phys. Rev. B 60 (1999) 16448.
[84] A.E. Mattsson, D.R. Jennison, Surf. Sci. 520 (1-2) (2002) L611, doi:10.1016/S0039-6028(02)02209-4.
[85] R. Armiento, A.E. Mattsson, Phys. Rev. B 72 (8) (2005) 085108.
[86] P. Wynblatt, R. Ku, Surf. Sci. 65 (2) (1977) 511.
[87] G. Treglia, B. Legrand, F. Ducastelle, A. Saul, C. Gallis, I. Meunier, C. Mottet, A. Senhaji, Comp. Mat. Sci. 15 (2) (1999) 196.
[88] M. Polak, L. Rubinovich, Surf. Sci. Rep. 38 (4–5) (2000) 127.
[89] J. Creuze, I. Braems, F. Berthier, C. Mottet, G. Tréglia, B. Legrand, Phys. Rev. B 78 (7) (2008) 075413, doi:10.1103/PhysRevB.78.075413.